



# Experimental and CFD Analysis on the Effect of Various Cold Orifice Diameters and Inlet Pressure of a Vortex Tube

N. Bagre<sup>†</sup>, A. D. Parekh and V. K. Patel

*Sardar Vallabhbhai National Institute of Technology, Surat, Gujarat, 395007, India*

<sup>†</sup>Corresponding Author Email: [ds18me008@med.svnit.ac.in](mailto:ds18me008@med.svnit.ac.in)

(Received April 30, 2022; accepted August 13, 2022)

## ABSTRACT

An experimental investigation was conducted to investigate the effects of different cold orifice diameters and operating pressures of the vortex tube. A vortex tube test rig was employed to conduct the experiments for various cold orifice diameters and operating pressures. Cold orifice diameters range from 1 mm to 6 mm, whereas the pressure condition ranges from 2 to 5 bar. The vortex generators were made up of brass material having six inlet nozzles. It was found that the temperature separation of the vortex tube significantly depends on the cold orifice diameter of the vortex tube and operating pressure. The study demonstrates the deviation of cold temperature separation with respect to the cold orifice diameters and inlet pressure for different cold mass fractions. In addition, present experimental results are used to determine the optimum cold orifice diameter, which is 5 mm at 5 bar inlet pressure. The percentage improvement in average cold temperature separation for 5 mm cold orifice diameter is 66.18% compared to rest of the cold orifice diameters at an inlet pressure of 5 bar. The maximum cooling power separation is 0.08 kW at 0.3 cold mass fraction and inlet pressure of 5 bar. The CFD technique was approached to discuss the complex fluid flow inside the tube at various radial distances. A three-dimensional numerical study was done and validated with the present experimental work. It was found that the numerical results are in good agreement with the present experimental data.

**Keywords:** Experimental analysis; Temperature separation; Cold orifice diameter; Inlet pressure; Cooling power separation; Vortex tube; CFD.

## NOMENCLATURE

$A_{\text{hot tube}}$	area of hot tube	$L$	tube length
CFD	Computational Fluid Dynamics	$P_{\text{inlet}}$	inlet pressure
COD	Cold Orifice Diameter	$P_{\text{cold}}$	pressure at cold exit
$D$	diameter of vortex tube	$Q_c$	cooling power separation
$D_{\text{inlet}}$	inlet diameter of nozzle	$\Delta T_{\text{cold}}$	temperature separation at cold outlet
$D_{\text{cold}}$	cold orifice diameter	$W_{\text{nozzle}}$	width of nozzle, mm
$H_{\text{nozzle}}$	height of nozzle	$\mu_c$	cold mass fraction
$L_{\text{tube}}$	hot tube length	3D	three-dimensional

## 1. INTRODUCTION

A thermal device which produces two different streams of hot and cold fluid at the exits of the tube is known as a Vortex tube. The high pressure working fluid is admitted tangentially via an inlet nozzle, which produces a swirling or vortex flow effect inside the tube. The temperature difference achieved by the fluid is because of its rotational flow mechanism, which leads to the formation of temperature separation phenomena. [Xue and Arjomandi \(2008\)](#) described the working principle of

flow separation inside the tube. Moreover, the flow characteristics like velocity, acoustic streaming, pressure, temperature, secondary circulation and turbulence were studied and discussed. The temperature separation phenomena without refrigerant or chemical reaction inside the tube always holds a keen interest of researchers to keep exploring this area. RHVT is simple in design with no moving parts, compact, easy to operate and maintenance free, but the flow separation mechanism is complex. The performance evaluation of the vortex tube is governed by the following parameters:

### 1.1 Cold Mass Fraction

It is the ratio of cold mass flow ( $\dot{m}_c$ ) of air at the cold junction to the inlet mass of compressed air ( $\dot{m}_a$ ). It is noteworthy that the fluctuation in cold mass fraction changes the magnitude of the temperature separation effect.

$$\mu_c = \frac{\dot{m}_c}{\dot{m}_a} \quad (1)$$

### 1.2 Cold Stream Temperature Difference

The inlet and cold outlet temperature difference define the temperature separation at the cold junction.

$$\Delta T_{Cold} = T_{inlet} - T_{Cold} \quad (2)$$

### 1.3 Hot Stream Temperature Difference

The temperature difference between the inlet air and the hot outlet air defines the temperature separation at the hot junction.

$$\Delta T_{hot} = T_{hot} - T_{inlet} \quad (3)$$

## 2. BACKGROUND

### 2.1 Effect of Nozzle Number

Rafiee and Rahimi (2013) carried out experimental and numerical work on the effects of nozzle convergence ratio, number of nozzles and inlet pressure on the vortex tube performance. It was found that the vortex tube performance can be improved by introducing a convergent nozzle. The magnitude of temperature drop increased in the cold region when the number of convergent nozzles increased. Li *et al.* (2015) experimentally studied the flow parting effect in a vortex tube. The static temperature was found low at the peripheral and high at the core of the tube. According to the study the stagnation point will move towards the cold region if the value of  $\mu_c$  increases or the inlet pressure decreases. A parametric analysis was performed by Nouri-Borujerdi *et al.* (2017) in which variables like nozzle number, vortex generator ratio and L/D ratio were studied. It is concluded that the L/D ratio dominates the performance of vortex tube as compared to the nozzle number.

### 2.2 Vortex Tube Design and Industrial Applications

Rahimi *et al.* (2013) replaced the circular tube with a divergent tube of RHVT and evaluated the performance at various divergent angles. The optimum divergent angle was found to be more than 4°, where it enhances the temperature separation effect at  $\mu_c \geq 0.4$ . The importance of vortex tubes in industrial applications was briefly discussed by Gutak (2015). It was observed that in an industry like the natural gas station, a vortex tube could be implemented for both heating and cooling purposes in a plant pipeline. A hybrid cooling, drying system was designed by Senturk Acar and Arslan (2017) using a vortex tube. The study examined R-134a as a working fluid and it was found that in summer, COP

and exergy efficiency was 0.0347 and 0.0094, and in winter it was 0.0409 and 0.0079 respectively. Yadav *et al.* (2016) worked on a vortex tube which had two cold and one hot exit. The investigation was done to find the effects of cold and hot end control plugs and the vortex tube performance at different cone angles. An investigation was carried by Pourmahmoud *et al.* (2015) to analyse the vortex tube performance considering various COD. The work concluded that better cooling effects can be achieved by an optimum COD of 4 mm. The utility of vortex tubes in industrial applications was discussed by Thakare and Parekh (2020). The results showed that a vortex tube using PA6 material can improve the vortex tube performance. The rate of cooling was increased by 10.47% as compared with mild steel at an inlet pressure condition of 4 bar. Dincer *et al.* (2009) utilized mobile plug locator of different diameters in a vortex tube at the hot exit and determined the performance of the tube. Here, the cross-sectional area of the hot outlet was varied while cold outlet was kept constant. It was concluded from the study that performance of the vortex tube can be elevated with 5 mm plug diameter and tip angle of 30° with four inlet nozzles considering air as a working fluid. Bazgir *et al.* (2018) utilized a double pipe RHVT to evaluate the effect on cooling rate. It was inferred from the study that the higher temperature separation could be obtained through a cooled hot tube having 4 nozzles with an L/D ratio of 47.5. Matveev and Leachman (2019) numerically investigated vortex tubes had a vortex chamber with an extension of cyclonic-type structure. The investigation stated that it performs well compared to the original system up to 15% of cold-flow fractions. Manimaran (2016) examined rectangular and trapezoidal geometries at inlet by changing the aspect ratio. The result found that the higher temperature separation could be achieved at high aspect ratio and also, the trapezoidal shape inlet delivered high-temperature separation as compared to the rectangular shape of the vortex tube. A numerical and experimental study of the convergent-divergent vortex tube by Zangana and Barwari (2020) showed that the cooling rate can be improved by convergent-divergent vortex tube.

### 2.3 Effect of Vortex Generator and Throttle Valve

Nimbalkar and Muller (2009) experimentally tested the various COD had different operating pressure and  $\mu_c$  of the vortex tube. The study concluded that the highest magnitude of temperature separation could be obtained by a specific COD. Rafiee and Sadeghiyazad (2014a) discussed the impacts of various parameters such as conical angle of the throttle valve, number of nozzles and operating pressure on the vortex tube effectiveness. According to the work maximum magnitude of the temperature separation could be obtained at a cone angle of 63° for the flow control valve of the vortex tube. Rafiee and Sadeghiyazad (2014b) had developed three-dimensional geometries to investigate the influence of throttle valve shape. Numerical work obtained using spherical shape throttle valve was compared with experimental work. Moraveji and Toghraie, (2017) examined various geometrical parameters

like nozzle number, length of the tube and cold orifice diameter. It indicated that if the L/D ratio increases, the fluid discharge also increases. [Thakare and Parekh \(2017\)](#) observed the influence of insulation on the performance of vortex tube and experimental data was utilized to develop a CFD model. The CFD results had good agreement with the experimental results. The details flow physics inside vortex tube was studied by developed CFD model. Also, it was concluded that by adding insulation to the vortex tube performance enhanced. An experimental and CFD work by [Rafiee \*et al.\* \(2015\)](#) investigated the convergent angle of the vortex tube and the optimum convergent angle was found to be 5° where the highest magnitude of temperature separation was achieved. In addition, the cooling rate was increased by 32.03% and heating rate increased by 26.21%. A RNG k-ε method was selected to determine the influence of curvature on the tube's performance by [Bovand \*et al.\* \(2014\)](#). [Zhai \*et al.\* \(2022\)](#) and [Ding and Zhou \(2022\)](#) introduced a new turbulence model discussing the detachment of eddy simulation considering non-linear eddy viscosity model. According to the study, the model is capable of solving the complex turbulent flow. In the study of [Jagos \*et al.\* \(2021\)](#) the influence of turbulent flow was discussed.

The aim of the present work is to study the effects of the cold orifice diameter and to improve the temperature separation effect by selecting an optimum COD. The work determines the cold orifice diameter of the vortex tube, which will provide the maximum magnitude of temperature separation which need in various engineering applications. Work also investigates the effect of various inlet pressures on the performance of vortex tube. According to the author's knowledge, such a study of cold orifice diameter was seldom testified, except for the investigation of [Nimbalkar and Muller \(2009\)](#). However, [Nimbalkar and Muller \(2009\)](#) performed experimental work with four nozzles and the range of diameters was 3.4 to 12.6 mm at various mass flow rates of 0.45, 0.68 and 0.82 kg/min. But in the present work distinguishing efforts are made to find the optimum COD using a different range of diameters i.e 1- 6 mm with six numbers of nozzle made up of brass material as shown in Fig. 4. The inlet pressure is varied in the range of 2-5 bars. In the present work, CFD analysis is also done to understand the flow physics of the vortex tube. It is evident from past research that the cold mass fraction provides a significant role in the temperature

separation magnitude. Therefore, a wide range of cold mass fractions was examined for various cold orifice diameters and inlet pressures. For engineering

applications other than cold temperature separation, the cooling power separation (Qc) is also significant. Hence in the present work, Qc is calculated at different cold mass fractions which is not reported by [Nimbalkar and Muller \(2009\)](#). Further, the next section deals with the computational study using present experimental data. A numerical simulation has been done by generating a 3D model of a vortex tube, further the results of the numerical and experimental work are compared. The epic ability of the CFD technique to visualise the fluid dynamics inside the tube helps the author to suggest the underlying flow physics of the vortex tube. Therefore, the core aims of the present study are:

1. To study cold temperature separation for various cold orifice diameters.
2. To obtain the optimum diameter based on maximum cold temperature separation.
3. To find the effect of cold orifice diameters,  $\mu_c$  and inlet pressure on cold temperature separation.
4. Compare present numerical results with experimental results for vortex tube parameters which give maximum temperature separation.
5. To find the cooling power separation for various cold orifice diameters.

### 3. EXPERIMENTAL SETUP

The instruments along with their statistical details used in the experimental vortex tube test rig are shown in Table 1. The schematic diagram of experimental test rig is illustrated in Fig. 1 and the

Instruments	Range	Resolution	Uncertainty
Rotameters	0-600 LPM	10 LPM	±1.99%
Thermocouples k-type	-19.9° to 200°C	0.1° C	±0.99%
Pressure Sensor	0 to 15.9 Bar	0.01 Bar	±0.2%

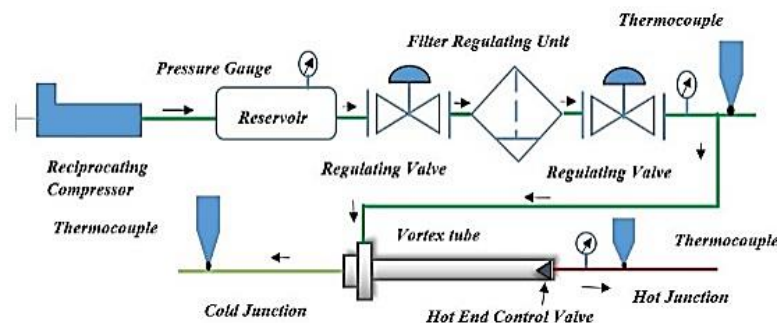


Fig. 1. Layout of test setup with the positioning of measuring instruments.

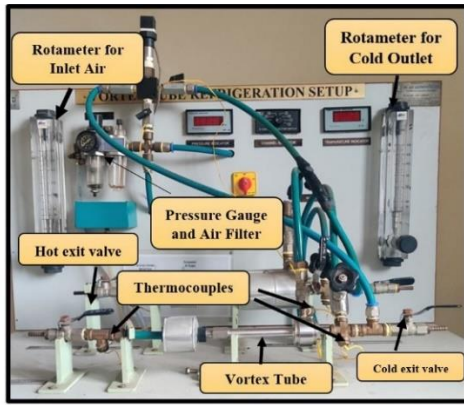


Fig. 2. Vortex tube test rig.

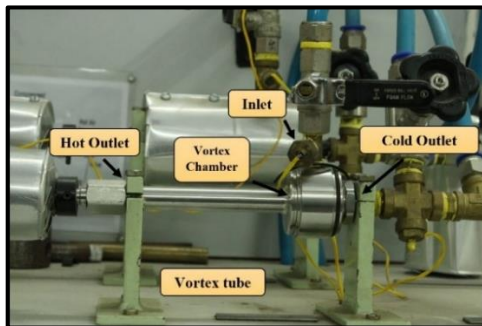


Fig. 3. Vortex tube.

actual test rig is shown in Fig. 2. The experiments were conducted using the pressure range of 2 to 5 bar and  $\mu_c$  of 0.1 to 0.9. A vortex tube model (Exair™ commercial VT Model No 3225, 708 slpm, 25 SCFM) used to conduct experiments in the present work is represented in Fig 3. In this experimental test rig, a two stage-reciprocating compressor was used to produce compressed air in order to operate the vortex tube. The apparatus is provided with a regulating valve and filter unit which is positioned after the reservoir to control the mass flow rate of air and to remove the moisture of the incoming compressed air.

The temperature of the fluid at the cold exit, hot exit and inlet was measured with the help of three thermocouples with an accuracy of  $\pm 0.1^\circ\text{C}$ . A pressure gauge was used to measure the pressure with an accuracy of  $\pm 0.01$  bar. The rotameters were used to measure the air flow rate at the inlet and cold outlet. To measure the temperature at a particular point, temperature probes are inserted into a hole having a diameter of 2 mm. The probes were placed in such a way that they aligned with the axis of the vortex tube and with a span of 10 mm apart from the hot and cold junctions shown in Fig. 3. The hole's cavities and probe are filled with the M-seal adhesive to avoid leakages. Before starting the experiment, all instruments are calibrated to avoid measurement errors and checked for air leakage using compressed air.

#### 4. PROCEDURE

The vortex tube test rig was started by providing the three-phases power supply to the reciprocating

compressor. To get the desired pressure, the filter regulating valve unit was opened. The hot and cold exit valves were kept fully opened initially. The compressor was run continuously until the tank reaches the pressure up to 10 kg/cm<sup>2</sup>. The supply of air must be continuing from the compressor throughout the experiment. The high pressurized air is directed to the vortex tube via a vortex generator to create the swirling flow within the vortex tube. Now, gradually close the exit valves to obtain the desired cold mass fraction. A minimum five minutes' time interval was given to reach a steady state condition for each desired cold mass fraction. Once the steady state condition has reached, the steady state temperature readings were noted down. After obtaining the set of readings at various cold mass fractions for one particular pressure, the same procedure is repeated for various inlet pressure. Before switching to other pressure, the complete test rig operation was shut down for a minimum 30 minutes so that the test-rig reached to room temperature. Experiments were repeated by using six vortex generators of different orifice diameters as shown in Fig. 4.

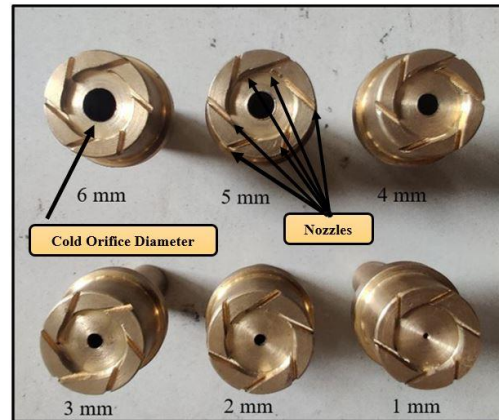
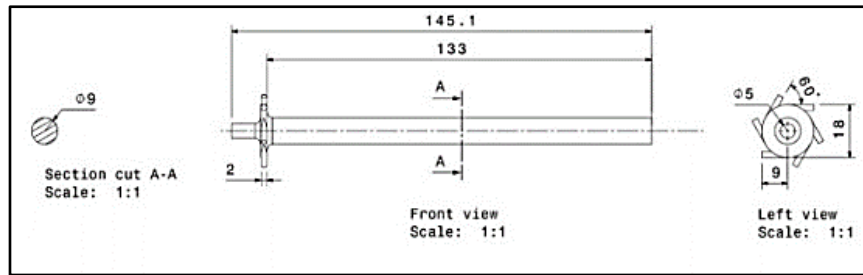


Fig. 4. Vortex generator with different orifice diameter used in testing for various pressure.

#### 5. ERROR AND UNCERTAINTY ANALYSIS

The details of the instruments used to measure the parameters are reported in Table 1. The parameters like pressure, temperature and flow rate of air were measured at the inlet and outlets of the vortex tube. Further, these observed values were used to calculate various vortex tube parameters i.e. cold stream temperature difference, cold mass fraction and cooling power separation. The authentication of methodology and apparatus can be justified by conducting an uncertainty analysis. So, an uncertainty analysis was conducted by adopting a Root Sum Square method (RSS) explained by Moffat (1988) and Abernethy *et al.* (1985). This method first includes a standard deviation of each parameter by,

$$\omega_{xi} = \sqrt{\frac{\sum_{i=1}^N (X_i - \bar{X})^2}{N - 1}} \quad (4)$$



**Fig. 5** Diagrammatic representation of circular vortex tube with specifications.

where,  $\bar{X}$  = Average values of observed values.

X = Observed values during the experiment

N = number of observations

i = index of parameter X .

$$R = f (x_1, x_2, x_3, \dots \dots \dots x_n, ) \quad (5)$$

Here the resultant value is represented by R as per Moffat (1988) and Abernethy *et al.* (1985). The independent variables like  $x_1, x_2, x_3, \dots \dots \dots x_n$  are the function of R. Let  $\omega_R$  represents the uncertainty in the result and  $\omega_1, \omega_2, \omega_3, \omega_4 \dots \dots \dots \omega_n$  represents uncertainties of independent variables. Now, the equation as per Moffat (1988) and Abernethy *et al.* (1985) to find the uncertainty is,

$$\omega_R = \left[ \sum_{i=1}^n \left( \frac{\partial R}{\partial X_i} \omega_{X_i} \right)^2 \right]^{1/2} \quad (6)$$

The uncertainty obtained through this method in the observed values of  $\Delta T_{cold}$ , cold mass fraction,  $m_i$ ,  $m_c$  and  $Q_c$  are  $\pm 1.412\%$ ,  $\pm 0.0912\%$ ,  $\pm 1.041$ ,  $\pm 0.8994\%$  and  $\pm 2.5871$  respectively.

## 6. GEOMETRICAL MODEL AND GRID

A 3D geometry of vortex tube was created with six inlet nozzles and two outlets. The dimensional parameters like area and length of the computational domain were kept same as the experimental apparatus. The computational domain specifications are given in Table 2. The high-pressure fluid was admitted tangentially via nozzles, which leads to the generation of turbulence inside the vortex tube.

**Table 2** Specification of the CFD domain

S.NO.	Parameters	Dimensions
1.	$L_{tube}$	133 mm
2.	$D_{inlet}$	10 mm
3.	$H_{nozzle}$	9 mm
4.	$W_{nozzle}$	2 mm
5.	$D_{cold}$	4 mm
6.	$A_{hot tube}$	63.61 mm <sup>2</sup>

The dimensions, computational domain and the generated mesh for the vortex tube are shown in Figs. 5, 6 and 7 respectively. A series of simulations were done with the help of FLUENT 18.2. Here, a density-

based solver was incorporated to discretize the governing equations such as continuity, momentum, and energy for the fluid. A second order equation was opted to evaluate the convective terms and to avoid the displacement terms. A SIMPLE scheme was selected to solve the turbulence equations.

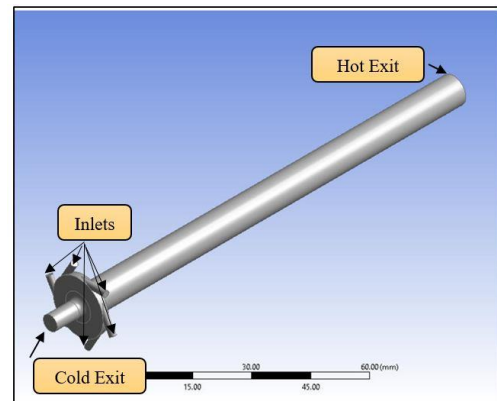


**Fig. 6** Vortex tube computational domain for simulation.

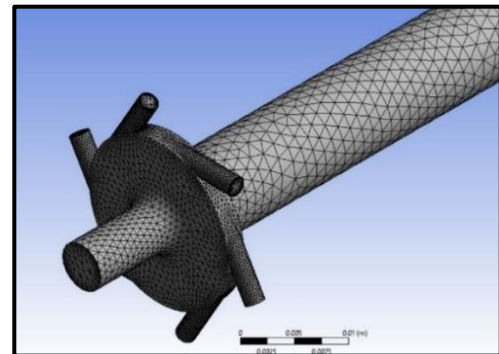


**Fig. 7.** Grid file of generated computational domain

## 7. GOVERNING EQUATIONS

Air is used as a working fluid considering it as compressible and Newtonian fluid, which resulted in the following equation and FLUENT 18.2 was used to discretize the equations.

### Continuity Equation

$$\frac{\partial}{\partial x}(\rho u) + \frac{\partial}{\partial y}(\rho v) + \frac{\partial}{\partial z}(\rho w) = 0 \quad (7)$$

### Energy Equation

$$\begin{aligned} \frac{\partial}{\partial x_i} \left[ u_i \rho \left( h + \frac{1}{2} u_i u_j \right) \right] \\ = \frac{\partial}{\partial x_j} \left[ k_{eff} \frac{\partial T}{\partial x_j} \right. \\ \left. + u_i (\tau_{ij})_{eff} \right] \end{aligned} \quad (8)$$

### Momentum Equation

$$\begin{aligned} \frac{\partial \rho (u_i u_j)}{\partial x_j} = - \frac{\partial p}{\partial x_i} + \frac{\partial}{\partial x_j} \left[ \mu \left( \frac{\partial u_i}{\partial x_j} + \frac{\partial u_j}{\partial x_i} \right. \right. \\ \left. \left. - \frac{2}{3} \delta_{ij} \frac{\partial u_k}{\partial x_k} \right) \right] \\ + \frac{\partial}{\partial x_j} (-\rho u_i' u_j') \end{aligned} \quad (9)$$

### Transport Equation For $k - \varepsilon$ Model

To solve the transport equation k-ε model, use two sets of equations they are as follows:

$$\begin{aligned} \frac{\partial}{\partial x_i} (\rho k u_i) = \frac{\partial}{\partial x_j} \left[ \left( \mu + \frac{\mu_t}{\sigma_k} \right) \frac{\partial k}{\partial x_j} \right] + G_k \\ + G_b - \rho \varepsilon - Y_M \\ + S_k \end{aligned} \quad (10)$$

$$\begin{aligned} \frac{\partial}{\partial x_i} (\rho \varepsilon u_i) = \frac{\partial}{\partial x_j} \left[ \left( \mu + \frac{\mu_t}{\sigma_k} \right) \frac{\partial \varepsilon}{\partial x_j} \right] \\ + C_{1\varepsilon} \frac{\varepsilon}{k} (G_k \\ + C_{3\varepsilon} G_b) - C_{2\varepsilon} \rho \frac{\varepsilon^2}{k} \\ + S_\varepsilon \end{aligned} \quad (11)$$

Here,

$G_k$ = Turbulence generation due to K.E.

$G_b$ = Turbulence generation due to buoyancy

$Y_m$ = Fluctuation behaviour during expansion.

$C_{1\varepsilon}, C_{2\varepsilon}$  &  $C_{3\varepsilon}$  are the constants

$\sigma_\varepsilon$  and,  $\sigma_k$  are the Prandtl number

## 8. BOUNDARY CONDITIONS

The boundary conditions were defined through the pressure conditions at the inlet and outlets. The compressed air admitted tangentially had a pressure of 5 bar. In numerical analysis, the mass flow rate at the exits was conserved by changing the hot exit pressure and maintaining the constant pressure at the cold stream which replicates the experimental conditions. In the experimental procedure, a hot exit valve controls the mass flow rate. The boundary conditions in the present numerical analysis are kept similar to the experimental conditions. In experimental methods, observations like temperature and cold mass fraction were recorded under steady state. Hence, a steady state condition was selected to examine all the simulations through an implicit solver which is pressure based. According to [Thakare et al. \(2015\)](#) k-ε turbulence model predicts the temperature separation consistently for all the cold mass fractions. Therefore, the standard k-ε turbulence model was utilized in the present numerical solver with a standard wall function. A

compressible flow develops inside the tube therefore, a density-based model with an ideal gas condition was assumed. A wall modelling was used in this case to enhance the wall treatment by providing inflation near the surfaces. The walls were selected as adiabatic wall with no heat loss and no-slip conditions. The convergence criteria for this numerical investigation are set up as  $10^{-4}$  for continuity, energy, and momentum equations.

## 9. RESULTS AND DISCUSSION

This section deals with the effect of COD on the vortex tube performance by evaluating the cold temperature separation at the various cold mass fractions. In the present experimental study total six cold orifice diameters i.e. 1 to 6 mm were selected to generate a pool of experimental data. It is difficult to visualize the flow mechanism inside the vortex tube hence to overcome this problem a CFD simulation was conducted. Subsequently, CFD simulation results are validated with experimental results. The entire work focuses on determining the optimum cold orifice diameter for the best possible temperature separation through experimental and CFD analysis. The cooling power separation parameter was also investigated to observe its influence over the performance of the system by using the following equation:

$$Q_c = m c_p (\Delta T_{cold}) \quad (12)$$

Where, mass flow rate is denoted by m

$C_p$  is the specific heat of air is  $1.006 \text{ kJ.kg}^{-1}.\text{K}^{-1}$

A 3D computational domain was created considering a COD of 5 mm because 5 mm COD achieved the highest magnitude of temperature separation in the present experimental study. The boundary condition of computational model had an operating pressure of 5 bar and outlets were open to the atmosphere. The desired magnitude of the cold mass fraction was obtained by controlling the pressure at the hot outlet. The flow characteristics like axial and swirl velocity, pressure, temperature, density and viscosity are also briefly discussed in this section.

## 10. EXPERIMENTAL RESULTS

### 10.1 Effect of Cold Orifice Diameter

The experiment was carried out with six different orifice diameters i.e. 1, 2, 3, 4, 5, 6 mm and six numbers of nozzles made up of brass material. Furthermore, a three-dimensional computational analysis was made and compared with the present experimental work to justify the computational results and also attempted to explain the flow physics inside the vortex tube.

### 10.2 Cold Temperature Separation

The present experimental results of temperature separation at the cold junction are shown in Fig. 8.1 to 8.4 for pressure ranges of 2 to 5 bar. The variation of temperature separation was studied at various cold mass fractions. Fig. 8.2 shows that, the results of the present investigation have a similar trend of  $\Delta T_{cold}$

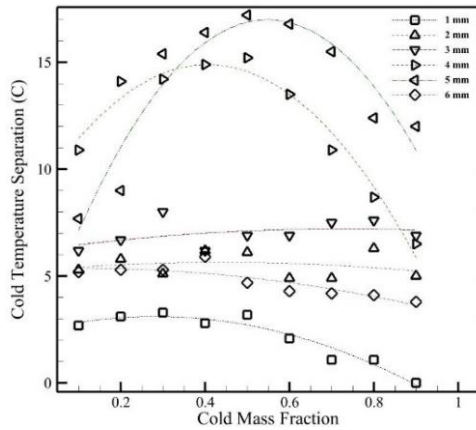


**Fig. 8.1.** Performance for different cold orifice diameters at Pinlet of 2 bar.

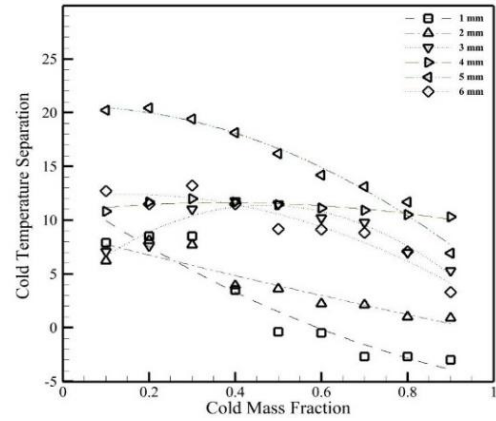


**Fig. 8.3.** Performance of different cold orifice diameters at Pinlet of 4 bar.

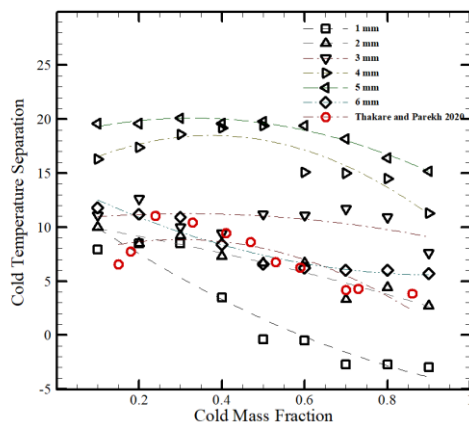


**Fig. 8.2.** Performance of different cold orifice diameters at Pinlet of 3 bar and results of (Thakare and Parekh, 2020).

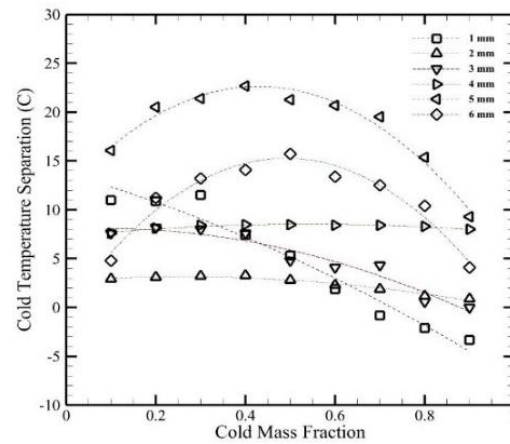


**Fig. 8.4.** Performance of different cold orifice diameters at Pinlet of 5 bar.

with cold mass fraction as observed in [Thakare and Parekh \(2020\)](#). It is observed from the results that the cold temperature separation drops when the cold mass fraction changes from 0.1 to 0.9 at all inlet pressure conditions. The temperature separation inside the tube was due to the structural flow mechanism. The compressed fluid was admitted tangentially, and it moves towards the end of the vortex tube, in which some partial amount of the fluid flows back towards the cold junction. This backflow of fluid towards the cold junction was governed by the cold orifice diameter. The diameter and the area of the vortex generator significantly affect both  $\Delta T_{\text{cold}}$  and  $Q_c$ . A high velocity magnitude of swirling flow was generated when fluid expanded due to the impulsive change in diameters of the vortex tube. There is a reduction in the intensity of the swirl velocity as the fluid moves towards the hot end. According to [Bej and Sinhamahapatra \(2014\)](#) a part of the cold stream reverses in the tube because of backflow and it mixes with the hot stream. Also, the secondary flow tends to mix with these fluids. The loss of energy is due to the mixing of these fluids, which generate energy in the form of vortices, heat, and momentum. The reason for temperature separation is due to the differences in the energy level of the system and surroundings. In this case, the

cold and hot exit was opened to the atmospheric pressure while inlet pressure was controlled by the compressor. This shows that, at the entrance, the energy level was high as compared to the exits. The above explanation gives an idea about how the cold end orifice influences the temperature separation inside the vortex tube. The maximum temperature separation was found with a 5 mm cold orifice diameter with an inlet pressure of 5 bar at 0.4 cold mass fraction. It can be observed that as the diameter increases, intensity of the backflow and mixing of fluids decreases which results in a lower magnitude of energy loss and generates high temperature differences.

Moreover, it can be observed that as the pressure increases, the relative magnitude of cold temperature separation increases at various cold mass fractions for all COD. It justified that cold orifice diameters dominate the flow separation between 0.4 - 0.6 cold mass fraction. According to [Ahlbom and Groves \(1997\)](#) the degradation of energy separation after  $\mu_c = 0.6$  is due to the existence of secondary circulation inside the tube indicating the mixing of flow (cold and hot). Furthermore, in the present work the presence of secondary flow was found due to reverse flow generated at the core of the tube, which is very high as compared to the cold mass flow

developed at the cold exit. The presence of secondary flow was reported inside the tube as shown in Fig. 9 which acts as a characteristic of cold orifice diameter.

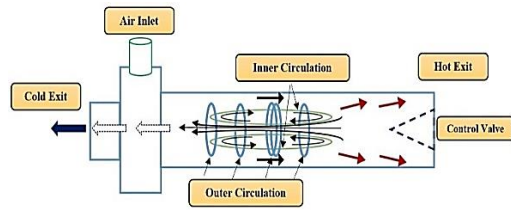


**Fig. 9. Line diagram of primary and secondary flow inside the vortex tube.**

In addition, [Poshernev and Khodorkov \(2003\)](#) also stated that the maximum magnitude of temperature separation and effectiveness of the vortex tube was found between 0.5–0.6 cold mass fraction. The results of the present experimental investigation also follow a similar trend, obtaining maximum performance at 0.6 cold mass fraction. Besides, the results show that after a specific cold orifice diameter, the magnitude of temperature separation starts decreasing in the present condition. This flow physics inside the tube could be understood by

applying the pressure balance, which is well described by [Love \(1974\)](#) and [Piralishvili and Fuzeeva \(2005\)](#).

### 10.3. Effect of Cooling Power Separation $Q_c$

Cooling power separation is one of the parameters to investigate the vortex tube's performance. The variation of cooling power separation of a vortex tube is discussed in this section. The variation of cooling power separation for various COD at different cold mass fraction is represented in Fig. 10.1 to 10.4. The value of specific heat of air was taken as  $1.006 \text{ kJkg}^{-1}\text{K}^{-1}$ . The highest magnitude of cooling power separation was found in the range of 0.5 - 0.8 cold mass fraction. The results showed similar trend observed during the investigation by [Skye \*et al.\* \(2006\)](#) of cooling power separation at  $P_{inlet} = 4.68 \text{ bar}$  as shown in Fig. 10.5. The cooling power separation showed a significant effect on the performance of the vortex tube. The magnitude of cooling power separation was low at the low cold mass fraction even though the temperature of air found low. This means the mass of cold air extracted was very less which shows that  $Q_c$  ought to be considered with cold temperature separation to evaluate the performance of vortex tube. It can be also concluded from Fig. 10.1 to 10.4 that the magnitude of cooling power separation increases as the inlet pressure increases.

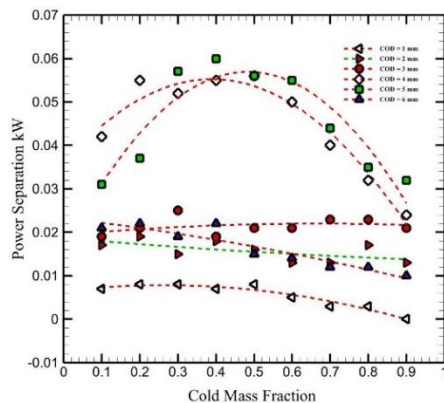


**Fig. 10.1. Cooling powers separation deviation along with cold mass fraction for inlet pressure of 2 bar.**

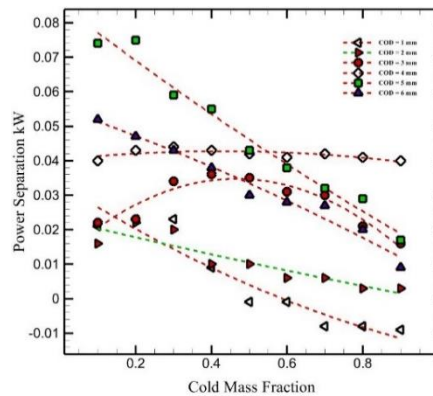


**Fig. 10.3. Cooling powers separation deviation along with cold mass fraction for inlet pressure of 4 bar.**

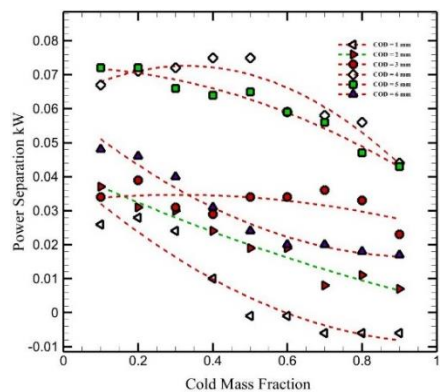


**Fig. 10.2. Cooling powers separation deviation along with cold mass fraction for inlet pressure of 3 bar.**

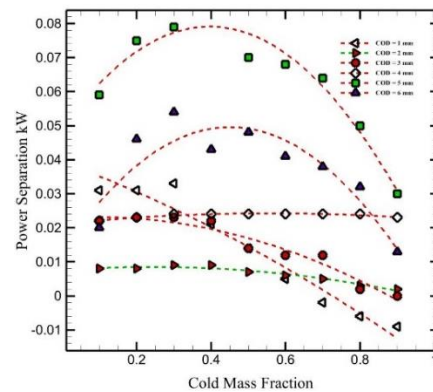


**Fig. 10.4. Cooling powers separation deviation along with different cold mass fraction for inlet pressure of 5 bar.**

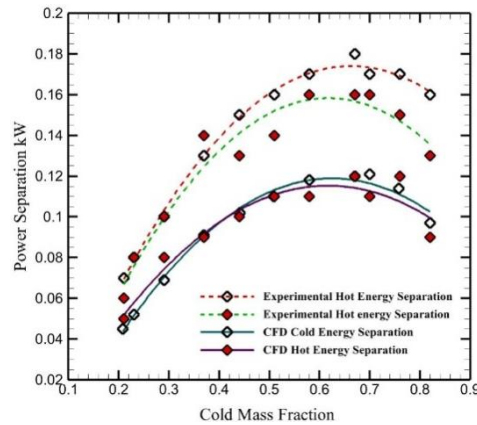


Fig. 10.5. Power separation deviation of (Skye *et al.* 2006) at  $P_{in} = 4.68$  bar.

#### 10.4 Effect of Various Inlet Pressure

To find an appropriate inlet pressure a study was carried out so that maximum temperature separation magnitude can be achieved through the vortex tube. It was observed as the pressure increases; the rate of temperature separation also increases as shown in Fig 8. The highest magnitude of temperature separation was found at 5 bar for the 5 mm COD of the vortex tube. Also, at an inlet pressure of 2 bar, the resultant magnitude of the temperature separation was low. The pressure drop at the vortex tube end elevated the volume of fluid and decreased the pressure. The friction between the walls and the fluid particles also causes a drop in pressure while moving towards the end of the tube. According to Prabhakaran *et al.* (2012) the temperature drop is directly proportional to the pressure drops, the more pressure drop causes higher temperature drop. The reason behind this phenomenon is the air, which is near the wall, causes high compression while the air at the core region generates expansion. Therefore, the surface of the tube has a high temperature while the core of the circulation is cold. The fluid particles start accelerating as the magnitude of operating pressure increases. The reason behind this increment of temperature separation with an increase in pressure is due to shear stress and friction developed inside the tube. This pressure gradient due to the wall friction and sudden expansion of air also degrades swirling flow vorticity inside the tube. Furthermore, this pressure gradient lowers the intensity of the axial velocity inside the tube. Also, the positioning of the axial stagnation point is decided through the pressure drop near the hot exit. The flow structure inside the tube depends on the pressure drop and the intensity of the swirl flow. The pressure drop defines the volume of the cold mass fraction, as the pressure gradient decreases, the axial stagnation point moves in the direction of the cold exit. This justification could be found in Adams *et al.* (1999) and Culick (1992) as they concluded that the flow structure highly depends on the pressure gradient taking place inside the vortex tube. The vortex tube is commonly used for cooling purposes as compared to heating. So, the work focuses more on increasing the rate of cooling. It is determined that as the pressure increases, the cooling rate also increases. But, it is not desirable economically. Therefore, it is required

to adjust the inlet pressure and to decide an operating pressure which achieves maximum cooling rate.

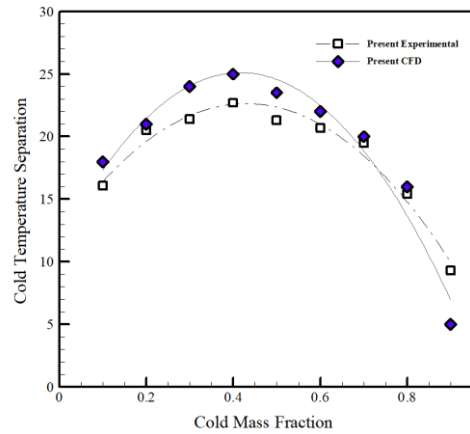
## 11. NUMERICAL RESULTS

### 11.1 Validation

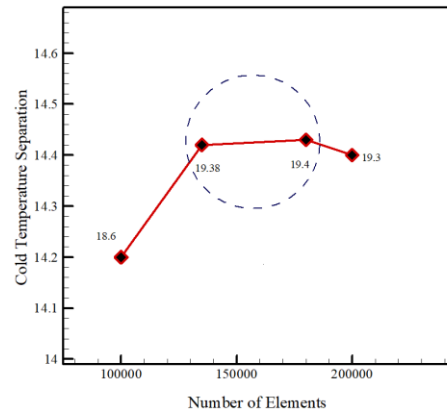
The results of the numerical simulation are validated with the present experimental results. The deviation between the numerical and experimental results is shown in Fig. 11(a) which represents cold temperature separation for different cold mass fractions. The operating pressure and the cold orifice diameter are taken 5 bar and 5 mm respectively in the computational study. A 3D computational domain was created considering similar dimensions which are used in the present experimental analysis. In both the experimental and numerical results, the highest cold temperature separation was found nearly at 0.4 cold mass fraction. Fig.11 (a) shows there is a good agreement between the computational and experimental results. Some variation in results may be attributed to the difference in boundary conditions and atmospheric conditions. Also, the inlet fluid is considered an ideal gas with no slip and walls to be adiabatic. The CFD method used can also predict the cold and hot end air temperature. There is some deviation was found due to the grid coarseness, which plays a significant role in CFD analysis. These errors can be minimized by conducting the grid independency test. In the present work, a grid independence test was conducted for the 1,00,000 to 2,00,000 elements as shown in Fig. 11(b). The influence of mesh density over the convergence and its stability could also be noticed. The grid independency test shows that the deviation of cold temperature separation between 1,30,000 to 1,80,000 number of elements was very less. So, the numerical simulation can be carried out within this grid range. Hence the present numerical simulation was carried out using 1,38,236 number of elements and 56,437 the number of nodes.

### 11.2. Flow Characteristic of Vortex Tube

The highest magnitude of the axial and tangential velocity was found in the cold peripheral. It was found that the air velocity drops in the vortex tube as it transfers towards the tube end. The maximum axial



(a)



(b)

**Fig. 11. (a) Computational and experimental results for an inlet pressure of 5 bar and COD of 5 mm (b) Grid size effect on cold temperature separation.**

and tangential velocity values were 130 m/s and 300 m/s respectively for 5 bar inlet pressure at 0.4 cold mass fraction. The difference between these two-velocity magnitudes can be observed in the Fig. 12 and Fig. 13. This shows that the tangential velocity dominates the flow inside the tube. The highest magnitude of velocity near the cold walls showed the presence of high kinetic energy coming from the inlet nozzle with high pressure. The fluid moves in the longitudinal direction with high kinetic energy and the intensity of flow decreases as it moves towards the end of the tube which shows a low magnitude of kinetic energy. The axial fluid velocity near the axis increases due to the expansion of gas. Figure 12 shows the behavior of axial velocity in which the positive region represents the hot temperature separation whereas the negative region shows the cold temperature separation.

However, the magnitude of axial and tangential velocity keeps on decreasing as it moves towards the wall of the tube. This shows the pressure gradient between the flow field and the cold junction. The pressure gradient is generated due to the fluid particles moving towards the hot junction. The resistive force obtained between the fluid particles and the pressure gradient acted on it as it transfers towards the end of the tube. This results in decreasing of axial velocity to zero magnitudes. The reason behind the temperature drop and elevating of axial velocity is due to the expansion of fluid particles that is continuously acted by the pressure gradient. In Fig. 14 the variation of static pressure with respect to the radial distance inside the tube can be noticed. Here, the maximum static pressure was found on the tube's wall while moving toward the hot exit the pressure gradient drops. This is due to the sudden air expansion, frictional and flow resistance with the wall. The resistive force drops the pressure towards the end of the tube and cause the sharp increase and decrease of velocity at the wall surfaces. The total temperature distributions are shown in Fig. 15 and 16 for the vortex tube. The highest and lowest total temperature values are 310 K and 276 K, respectively. The reason behind the total temperature

elevated at the tube's end and dropped at the cold end was due to the low kinetic energy.

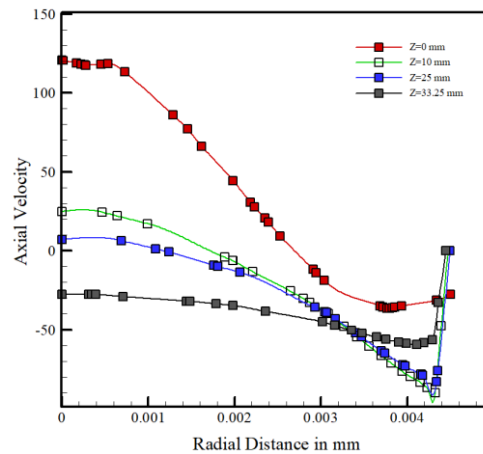


**Fig. 12. Axial velocity distribution along the radial distance.**

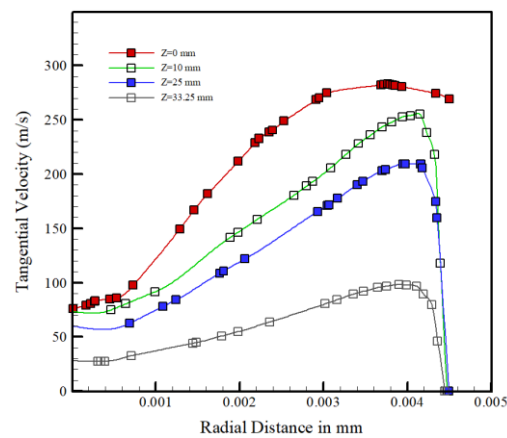


**Fig. 13. Tangential velocity distribution along the radial distance.**

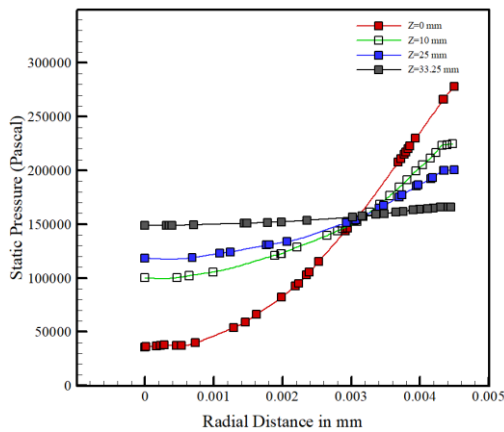


**Fig. 14. Variation of static pressure along the radial distance of vortex tube.**

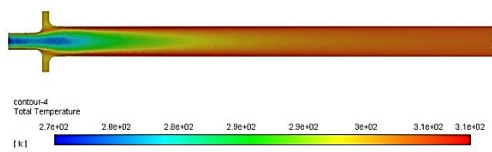


**Fig. 15. Total temperature distribution contour inside the vortex tube.**

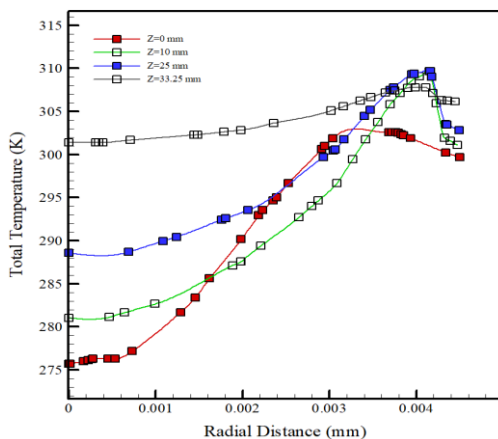


**Fig. 16. Variation of total temperature along the radial distance.**

Figure 16 shows the variation of total temperature along the radial distance of vortex tube. The compressed air with high pressure has immense kinetic energy that generates the swirling flow effect

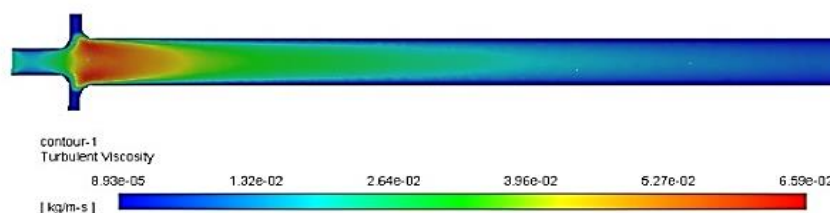


**Fig. 17. Turbulent viscosity contour inside the vortex tube.**

inside the tube. It was observed that, due to radial pressure and kinetic energy, the temperature separation effect was developed. The kinetic energy was falling from the centre to the wall along axial direction of the tube due to the sudden expansion of air. The air expands in the longitudinal direction close to the hot exit where the particles of air generates the thermal energy. Hence, as the temperature rises along the longitudinal length and velocity demote, this transformation of kinetic energy into thermal energy is due to the shear effect. Further, the fluid characteristics play a significant role in temperature separation. These fluid characteristics are density and viscosity. The temperature separation occurs due to a high-density gradient which results in a strong centrifugal force that generates inside the tube. The energy separation is due to this density gradient. The turbulent viscosity defines the intensity of turbulence when the fluid flow inside the tube. Here, the molecular viscosity is dominated by turbulent viscosity in highly turbulent and swirling flow field inside the tube. It was observed that as the flow progresses towards the end of the tube the magnitude of turbulent viscosity decreases. Fig. 17 shows that the turbulent viscosity is high near the entrance of the vortex tube and as flow moves towards the end of the tube, its effect dissipates. It is almost negligible in the second half of the vortex tube which cause the sudden change in static temperature.

## 12. CONCLUSION

The present work deals in two parts, i.e. experimental and numerical. The first part was carried out with an experimental investigation of vortex tube considering various cold orifice diameters. In addition, the cooling power separation was investigated to determine the optimum diameter of the cold orifice for various engineering applications. It is found that the maximum magnitude of temperature separation can be obtained using a 5 mm cold orifice diameter. Further, the flow physics inside the vortex tube was described by performing a numerical simulation. A 3D CFD analysis was done for a 5 mm cold orifice diameter of a vortex tube. The study shows satisfactory results with the present experimental results. The flow mechanism inside the vortex tube has also been discussed. The conclusions of the present work are as follows:

1. The overall estimation of cold temperature separation by numerical work is in good agreement with present experimental work.

2. The maximum rise of cold temperature separation is found in 5 mm cold orifice diameter. Therefore, the optimum cold orifice diameter is 5 mm among various diameters considered in the present study.

3. The experimental results show that, when the cold orifice diameter is less than 5 mm, the magnitude of temperature separation is very low even at a high inlet pressure of 5 bar. It is found that the average rise in cold temperature separation at COD of 5 mm is 66.18% compared with the rest of the diameters.

4. The cooling power separation indicates that the highest cooling rate is found in a 5 mm cold orifice diameter. For the same cold orifice diameter, cooling power separation increases with increase in the inlet pressure.

5. A 3D numerical simulation flow mechanism inside the vortex tube has been explored. The flow characteristics like axial velocity, tangential velocity, static pressure, density and viscosity affecting temperature separation inside the vortex tube has been discussed.

#### ACKNOWLEDGEMENT

Authors would like to show gratitude to TEQIP-III of Government of India and SVNIT, Surat for granting fund via. MED/PhD/2052/2019-20 for this research work.

#### REFERENCES

Abernethy, R. B., R. P. Benedict and R. B. Dowdell (1985). Asme Measurement Uncertainty. *Journal of Fluids Engineering* 107(2), 161-164.

Adams, B., M. Jones, K. Hourigan, M. Thompson (1999). Hysteresis in the open pipe flow with vortex breakdown. *2nd International Conference on CFD in the Minerals and Process Industries CSIRO, Melbourne, Australia 6-8 December 1999* Process Ind. 311-316.

Ahlbom, B. and S. Groves (1997). Fluid Dynamics Secondary flow in a vortex tube. *Fluid Dynamics Research* 21, 73-86.

Bazgir, A., N. Nabhani, S. Eiamsa-ard (2018). Numerical analysis of flow and thermal patterns in a double-pipe Ranque-Hilsch vortex tube: Influence of cooling a hot-tube. *Applied Thermal Engineering* 144, 181-208.

Bej, N. and K. P. Sinhamahapatra (2014). Exergy analysis of a hot cascade type Ranque-Hilsch vortex tube using turbulence model. *Energy Economics* 45, 13-24.

Bovand, M., M. S. Valipour, K. Dincer, A. Tamayol (2014). Numerical analysis of the curvature effects on Ranque-Hilsch vortex tube refrigerators. *Applied Thermal Engineering* 65, 176-183.

Culick, F. E. C. (1992). The role of non-uniqueness

in the development of vortex breakdown in tubes. *Journal Fluid Mechanics* 242, 491-527.

Dincer, K., S. Baskaya, B. Z. Uysal and I. Ucgul (2009). Experimental investigation of the performance of a Ranque-Hilsch vortex tube with regard to a plug located at the hot outlet. *International Journal of Refrigeration* 32, 87-94.

Ding, P. and X. Zhou (2022). A DDES Model with Subgrid-scale Eddy Viscosity for Turbulent Flow. *Journal of Applied Fluid Mechanics* 15, 831-842.

Gutak, A. D. (2015). Experimental investigation and industrial application of Ranque-Hilsch vortex tube. *International Journal of Refrigeration* 49, 93-98.

Jagos, J., J. Kohut, M. Kotek, P. Skacel and J. Bursa (2021). Influence of Turbulence in Aorta-like Tube: Computational and Experimental Study. *Journal of Applied Fluid Mechanics* 14, 1411-1420.

Li, N., Z. Y. Zeng, Z. Wang, X. H. Han and G. M. Chen (2015). Experimental study of the energy separation in a vortex tube. *International Journal of Refrigeration* 55, 93-101.

Love, W. J. (1974). Prediction of Pressure Drop in Straight Vortex Tubes. *AIAA Journal* 12, 959-965.

Manimaran, R. (2016). Computational analysis of energy separation in a counter-flow vortex tube based on inlet shape and aspect ratio. *Energy* 107, 17-28.

Matveev, K. I. and J. Leachman (2019). Numerical investigation of vortex tubes with extended vortex chambers. *International Journal of Refrigeration* 108, 145-153.

Moffat, R. J. (1988). Describing the uncertainties in experimental results. *Experimental Thermal And Fluid Science* 1, 3-17.

Moraveji, A. and D. Toghraie (2017). Computational fluid dynamics simulation of heat transfer and fluid flow characteristics in a vortex tube by considering the various parameters. *International Journal Heat Mass Transfer* 113, 432-443.

Nimbalkar, S. U. and M. R. Muller (2009). An experimental investigation of the optimum geometry for the cold end orifice of a vortex tube. *Applied Thermal Engineering* 29, 509-514.

Nouri-Borujerdi, A., M. Bovand, S. Rashidi, K. Dincer (2017). Geometric parameters and response surface methodology on cooling performance of vortex tubes. *International Journal Of Sustainable Energy* 36, 872-886.

Piralishvili, S. A. and A. A. Fuzeeva (2005). Hydraulic characteristics of ranque-hilsch

- energy separators. *High Temperature* 43, 900–907.
- Poshernev, N. V. and I. L. Khodorkov (2003). Experience from the operation of a conical vortex tube with natural gas. *Chemical And Petroleum Engineering* 39, 602–607.
- Pourmahmoud, N., R. Esmaily and A. Hassanzadeh (2015). Experimental investigation of diameter of cold end orifice effect in vortex tube. *Journal Thermophysics and Heat Transfer* 29, 629–632.
- Prabakaran, J., S. Vaidyanathan and D. Kanagarajan (2012). Establishing empirical relation to predict temperature difference of vortex tube using response surface methodology. *Journal of Engineering Science Technology* 7, 722–731.
- Rafiee, S. E. and M. Rahimi (2013). Experimental study and three-dimensional (3D) computational fluid dynamics (CFD) analysis on the effect of the convergence ratio, pressure inlet and number of nozzle intake on vortex tube performance-Validation and CFD optimization. *Energy* 63, 195–204.
- Rafiee, S. E. and M. M. Sadeghiazad (2014a). Effect of conical valve angle on cold-exit temperature of vortex tube. *Journal Thermophysics and Heat Transfer* 28, 785–794.
- Rafiee, S. E. and M. M. Sadeghiazad (2014b). Three-dimensional and experimental investigation on the effect of cone length of throttle valve on thermal performance of a vortex tube using k- $\epsilon$  turbulence model. *Applied Thermal Engineering* 66, 65–74.
- Rafiee, S. E., M. M. Sadeghiazad and N. Mostafavinia (2015). Experimental and numerical investigation on effect of convergent angle and cold orifice diameter on thermal performance of convergent vortex tube. *Journal of Thermal Science and Engineering Applications* 7(4).
- Rahimi, M., S. E. Rafiee and N. Pourmahmoud (2013). Numerical investigation of the effect of divergent hot tube on the energy separation in a vortex tube. *International Journal of Heat Technology* 31, 17–26.
- Senturk, Acar, M. and O. Arslan (2017). Exergo-economic Evaluation of a new drying system Boosted by Ranque-Hilsch vortex tube. *Applied Thermal Engineering* 124, 1–16.
- Skye, H. M., G. F. Nellis and S. A. Klein (2006). Comparison of CFD analysis to empirical data in a commercial vortex tube. *International Journal of Refrigeration* 29, 71–80.
- Thakare, H. R., A. Monde, B. S. Patil, A. D. Parekh (2015). Numerical Investigation of Flow Characteristics in Counter Flow Vortex Tube. *Procedia Engineering* 127, 170–176.
- Thakare, H. R. and A. D. Parekh (2017). Experimental investigation & CFD analysis of Ranque–Hilsch vortex tube. *Energy* 133, 284–298.
- Thakare, H. R., A. D. Parekh (2020). Experimental investigation of Ranque — Hilsch vortex tube and techno – Economical evaluation of its industrial utility. *Applied Thermal Engineering* 169, 114934.
- Xue, Y. and M. Arjomandi (2008). The effect of vortex angle on the efficiency of the Ranque-Hilsch vortex tube. *Experimental Thermal and Fluid Science* 33(1), 54–57.
- Yadav, G. M. P., P. M. Reddy, B. U. M. Gowd (2016). Effect of end control plugs on the performance of Vortex tube with dual forced vortex flow. *Journal of Thermal Engineering* 2, 871–881.
- Zangana, L. M. K. and R. R. I. Barwari (2020). The effect of convergent-divergent tube on the cooling capacity of vortex tube: An experimental and numerical study. *Alexandria Engineering Journal* 59, 239–246.
- Zhai, L. J., H. X. Chen, Z. Ma (2022). A Delayed Detached Eddy Simulation Model for the Simulation of Complex Turbulent Flow. *Journal of Applied Fluid Mechanics* 15, 1111–1124.